Degenerate mapping of environmental location presages deficits in object-location encoding and memory in the 5xFAD mouse model for Alzheimer's disease

Hai Zhang[a], **Lujia Chen**[a,b], **Kevin G. Johnston**[c], **Joshua Crapser**[d], **Kim N. Green**[d,h], **Nicole My-Linh Ha**[a], **Andrea J. Tenner**[e], **Todd C. Holmes**[f,h], **Douglas A. Nitz**[g,h,**], **Xiangmin Xu**[a,b,h,*]

[a]Department of Anatomy and Neurobiology, School of Medicine, University of California, Irvine, CA 92697, United States of America

[b]Department of Biomedical Engineering, University of California, Irvine, CA 92697, United States of America

[c]Department of Mathematics, University of California, Irvine, CA 92697, United States of America

[d]Department of Neurobiology and Behavior, School of Biological Sciences, University of California, Irvine, CA 92697, United States of America

[e]Department of Molecular Biology and Biochemistry, School of Biological Sciences, University of California, Irvine, CA 92697, United States of America

[f]Department of Physiology and Biophysics, School of Medicine, University of California, Irvine, CA 92697, United States of America

[g]Department of Cognitive Science, University of California, San Diego, La Jolla, CA 92093, United States of America

[h]Center for Neural Circuit Mapping, University of California, Irvine, CA 92697, United States of America

Abstract

A key challenge in developing diagnosis and treatments for Alzheimer's disease (AD) is to detect abnormal network activity at as early a stage as possible. To date, behavioral and neurophysiological investigations in AD model mice have yet to conduct a longitudinal assessment

*Correspondence to: Xiangmin Xu, Department of Anatomy and Neurobiology, School of Medicine, University of California, Irvine, CA 92697-1275, United States of America. xiangmix@uci.edu (X. Xu). **Correspondence to: Douglas A. Nitz, Department of Cognitive Science, University of California, San Diego, La Jolla, CA 92093, United States of America. dnitz@ucsd.edu (D.A. Nitz).

of cellular pathology, memory deficits, and neurophysiological correlates of neuronal activity. We therefore examined the temporal relationships between pathology, neuronal activities and spatial representation of environments, as well as object location memory deficits across multiple stages of development in the 5xFAD mice model and compared these results to those observed in wild-type mice. We performed longitudinal in vivo calcium imaging with miniscope on hippocampal CA1 neurons in behaving mice. We find that 5xFAD mice show amyloid plaque accumulation, depressed neuronal calcium activity during immobile states, and degenerate and unreliable hippocampal neuron spatial tuning to environmental location at early stages by 4 months of age while their object location memory (OLM) is comparable to WT mice. By 8 months of age, 5xFAD mice show deficits of OLM, which are accompanied by progressive degradation of spatial encoding and, eventually, impaired CA1 neural tuning to object-location pairings. Furthermore, depressed neuronal activity and unreliable spatial encoding at early stage are correlated with impaired performance in OLM at 8-month-old. Our results indicate the close connection between impaired hippocampal tuning to object-location and the presence of OLM deficits. The results also highlight that depressed baseline firing rates in hippocampal neurons during immobile states and unreliable spatial representation precede object memory deficits and predict memory deficits at older age, suggesting potential early opportunities for AD detecting.

Keywords

Animal model; hippocampus; CA1; Object location memory; Spatial encoding; Disease progression; Neural circuit; Alzheimer's disease

1. Introduction

A key challenge in developing diagnosis and treatments for Alzheimer's disease (AD) is to detect neurophysiological deficits as early as possible. AD neuropathology appears to precede measurable cognitive impairments in AD patients by years or even decades, but the predictive value of such neuropathological markers is still controversial (Jack et al., 2013). In recent years, studies suggest that deficits in neural circuit activity better predict the progressive impairments of spatial memory and spatial navigation (Canter et al., 2016; Iaccarino et al., 2016; Veitch et al., 2018; Harris et al., 2020; Dautricourt et al., 2021). However, the neural circuit mechanisms underlying the progressive developing of spatial navigation and memory deficits are not fully understood, and the temporal relationship between impaired neural circuit mechanisms and memory performance in AD remain unclear. Understanding the relative timing of circuit-level versus memory deficits is critically important for developing early detection and intervention for AD.

The CA1 region of the hippocampus is critical for spatial navigation and cognition as, for example, in object location memory (Assini et al., 2009; Barrett et al., 2011; Sun et al., 2019). Object location memory (OLM) deficits have been reported in aged mice, elderly individuals and AD patients (Murai et al., 2007; Muffato et al., 2019; Zokaei et al., 2020). CA1 pyramidal neurons exhibit tuning of their activity to environmental locations (i.e., places) and are commonly referred to as "place cells". The maintenance of place-specific firing patterns among CA1 neuron populations is thought to be key to spatial cognition and

memory formation (O'Keefe and Dostrovsky, 1971; McHugh et al., 1996; Kentros et al., 1998; Henriksen et al., 2010), and stable mapping during revisiting of the same environment supports spatial memory (Muller et al., 1987; Barnes et al., 1997). In AD models, functional imaging of CA1 place cells has revealed impaired neural circuit features, including unstable place fields, degraded spatial representation and disrupted place cell remapping (Cacucci et al., 2008; Cheng and Ji, 2013; Mably et al., 2017; Jun et al., 2020; Lin et al., 2022). However, most current studies focus on the deficits at discreet time points rather than addressing the presumed longitudinal progression of disease, thus the temporal relationship between the appearance of neural circuit and memory deficits has yet to be studied.

Hippocampal activity is organized by theta oscillations during locomotor states, or organized into bursts associated with sharp wave ripples (SWRs) during immobile states, which are key components of memory consolidation (Buzáski et al., 1992; O'Neill et al., 2008; Dupret et al., 2010). In transgenic AD models, both increased and decreased activity of hippocampal CA1 pyramidal neurons have been reported (Busche et al., 2012; Mably et al., 2017; Sompol et al., 2017; Lin et al., 2022), suggesting that overall measures of population activity may not be optimal in predicting cognitive decline. Furthermore, as reduced rates may reflect either linear declines in overall activity or more intermittent failures in firing for individual neurons, measures of reliability in spatial tuning across repeated experience are needed to provide insight into how failures in co-activation of connected neurons can link reduced rates to memory encoding failures (McHugh et al., 1996; Iaccarino et al., 2016; Sun et al., 2019). Thus, we propose that locomotion- and task related measures of firing rate and neural tuning reliability may provide new insight into the means by which rate changes relate to impairments in memory encoding and consolidation (Sun et al., 2019).

We recently applied miniscope imaging to behaving AD model mice, and demonstrated spatial coding defects in hippocampal neural calcium ensembles in the triple-transgenic AD model (3xTg-AD) (Lin et al., 2022). Based on our established feasibility, for the present study, we aim to address the neural mechanism underlying AD progression by examining the temporal relationship between behavioral memory performance and the onset and degree of neural circuit activity alterations. Leveraging the strengths of 5xFAD mouse model, we longitudinally measured the hippocampal CA1 ensemble calcium activity during behavior tasks in the same cohorts of 5xFAD model and wild type control mice during 4 to 14-month-old. The 5xFAD mouse model carries 3 mutations in human amyloid precursor protein and 2 mutations in presenilin 1, inducing early and rapid amyloid aggregation before the emergence of memory deficits (Oakley et al., 2006; Girard et al., 2014; Forner et al., 2021). 5xFAD mice recapitulate memory impairments that resemble AD (Oakley et al., 2006; Kimura and Ohno, 2009; Girard et al., 2014; Caccavano et al., 2020). We find that 5xFAD mice develop amyloid plaques, depressed neuronal activity during immobile states, and degenerate and unreliable spatial tuning at very early stages (by 4 months of age) with intact object location memory, recapitulating a critical feature of human AD that pathology emerges far earlier than cognition impairment. Object location memory deficits appear at 8 months old, accompanied by progressive degeneration of spatial representation and impaired CA1 ensemble patterns discriminating to object-location pairings. Furthermore, depressed neuronal activity and unreliable spatial encoding at early stage are correlated with impaired performance in OLM at 8-month-old. Our study indicates that early onset of degenerate

neural activity and unreliable spatial representation precede OLM deficits in AD, and these impairments in circuit activities at early stage predict OLM deficits at older age, suggesting potential early opportunities for AD detection.

2.   Materials and methods

2.1.   Mice

5xFAD mice and their wild type (WT) littermates were obtained from the Model Organism Development and Evaluation for Late-onset Alzheimer's Disease (MODEL-AD) center at the University of California, Irvine. Mice were housed under controlled environment with temperature maintained at 21–23 °C and humidity at 40% - 70%. Mice had free access to water and diet except water restriction during linear track test. The age was 2–3 months at the beginning of the experiment, both sexes were included. For a great majority of the data analysis, we pooled female and male mouse data for analysis since we did not observe major sex-related differences of behavior and calcium activity data between aged-matched male and female control or 5xFAD mice. Please see Supplementary Fig. S1 for OLM behavior data, Fig. S2 for calcium activity data and Figs. S3–S4 for some key features of spatial encoding properties split by sex. All the experimental protocols were approved by the IACUC of the University of California, Irvine and carried out in accordance with the Guide for the Care and Use of Laboratory Animals of the US National Institutes of Health.

2.2.   Virus injection

Surgery was performed as described previously (Sun et al., 2019; Lin et al., 2022). Briefly, AAV1-CaMKIIa-GCaMP6f-WPRE-SV40 was purchased from Addgene. Mice were anesthetized with 1.5% - 2% isoflurane and placed on a stereotaxic instrument (Stoelting). A micromanipulator guided by a digital atlas was used to determine coordinates for the bregma and lambda. The virus was injected into dorsal CA1 (AP −1.94, L 1.4, DV −1.38 mm, relative to the bregma) of the right hemisphere using a glass micropipette. We recorded from the right hippocampus as the right side of the brain tends to be more related to processing spatial information (Shinohara et al., 2012; Lin et al., 2022). A 0.5-mm-diameter hole was drilled in the skull above the injection site. The diameter of the pipette tip was 20–30 μm. The virus titer was 1×10^{13} GC/ml and injection volume was 0.3 μl. Virus was infused at speed of 0.1 μl /min by short pulses of air pressure (PICOSPRITZER III). The glass pipette remained in place for 5 min before being withdrawn. Mice were treated with carprofen (3 mg/kg) as analgesia for 3 days after surgery.

2.3.   GRIN lens implantation

To record CA1 neurons, a GRIN lens was implanted at two weeks after virus injection (Sun et al., 2019). Mice were anesthetized with isoflurane, and carprofen and dexamethasone (2 mg/kg) were administered. A craniotomy of 2-mm-diameter was performed over CA1, centered at AP −2.3, L 1.75 mm. Then dura was removed with ultrafine forceps, and the cortical tissue above the target CA1 area was carefully aspirated using a 29-G blunt needle connected to vacuum, until the vertical striations of corpus callosum appeared. Sterile saline was continuously applied during aspirating. After bleeding being completely stopped, a GRIN lens (1.8 mm diameter, 4.3 mm length, 0.25 PITCH, Edmund Optics) was lowered

to contact the corpus callosum (depth – 1.55 mm) for CA1 imaging, and secured with superglue and dental cement. The skull and lens were covered with Kwik-Sil silicone elastomer (WPI) and mice were allowed to recover for 2–3 weeks.

Mice were anesthetized again, Kwik-Sil was removed and a miniscope (UCLA) mounted onto a baseplate was placed on the GRIN lens to search the imaging area. After cells being in focus, the baseplate was attached on the skull with dental cement, the miniscope was removed and a plastic cap was placed on the baseplate to prevent dust.

2.4. In vivo calcium imaging in free moving mouse

Calcium activity of CA1 neurons during the following behavioral tests was recorded by miniscope, and mouse behavior was recorded by a Logitech webcam simultaneously. Tests were performed starting at the age of 4–5 months, and most of the mice were repeatedly tested at 8–10 months and some of them were further tested at14 months when possible (Supplementary table 1). Mice were handled and habituated with miniscope tethering before tests.

1. object location memory (OLM): mice were habituated in a 22×28 cm chamber with visual cues on its walls for 10 min per day for 3 days. In training session, two identical objects were placed in the chamber and each mouse was allowed to explore the box for 10 min. Testing session was performed at 24 h after training, in which one object was moved to a new location and the other remained the initial location. Mice were placed in the box and explored for 10 min. The chamber and objects were cleaned with 70% ethanol before each session. Exploring time on each object was calculated by an experimenter blinded to grouping. Discrimination index (DI) in testing session was calculated as (Time moved object – Time unmoved object)/ (Time moved object + Time unmoved object). Mouse data were excluded if the total exploring time on the 2 objects was <5 s. To repeatedly test the same cohort of mice, different chambers and different sets of objects were used at different time points.

2. open field: mice were habituated in a circle box (diameter of 28 cm) and a square box (25 cm $\times$ 25 cm) for 3 days, 10 min in each box each day. Visual cues were attached on the box walls. The box floor was covered by corn cob bedding, the bedding was not changed throughout the whole habituation and recording sessions, but feces was removed and the bedding was shaken before each session to equally distribute any odor cues. The test included two sessions per day and was repeated for 4 days. On the first day mice were placed in the circle box for 10 min then in the square box for another 10 min, and the order of box exploring was alternated on each following day.

3. linear track: mice were water restricted until their bodyweight reached 85% - 90% of the initial weight (it took 3–5 days), then they were trained to run back and forth on a 1-m-long linear track to obtain 10–20 μl of water reward on either end of the track. After 5 days of training, miniscope was tethered and mice were trained for another 5 days. The testing consisted of two sessions at 30 min apart each day and was repeated for 3 days. On the first day, the linear track

was placed in the initial orientation of training. On the second day, the track remained the initial orientation in the first session, and rotated for 90 degrees in the second session. On the third day, the orientation was 90-degree rotated in the first session and back to the initial orientation in the second session. Mice were recorded for 30 trials (laps) in each session, usually finishing in 10–15 min. Linear track was cleaned with 70% ethanol before each recording.

2.5. Immunohistochemistry

Post hoc histology was conducted to confirm AAV expression, location of GRIN lens implantation and amyloid aggregations. Mice were deeply anesthetized with isoflurane and perfused with cold PBS followed by 4% paraformaldehyde (PFA). Brains were dissected and further fixed in 4% PFA for 24 h, cryoprotected in 30% sucrose and cut into 40 μm coronal sections. For amyloid staining, free floating brain sections were blocked in PBS containing 5% normal donkey serum and 0.1% Triton X-100. Then sections were incubated in amyloid antibodies (6E10, BioLegend) overnight at 4 °C. Sections were washed 3 times in PBS and incubated in secondary antibodies for 1 h at room temperature. Sections were washed 3 times in PBS, stained with DAPI and mounted. Images were taken under an Olympus FV3000 confocal microscope.

2.6. Evaluation of amyloid pathology

To evaluate the progression of amyloid pathology in this model, a different set of mice (age 4, 8 and 12 months) were euthanized via CO_2 inhalation and transcardially perfused with ice-cold PBS. Brains were removed, and hemispheres were separated along the midline. Each hemisphere was then drop-fixed in 4% PFA for 48 h, cryoprotected in 30% sucrose +0.05% sodium azide, and sectioned at 40 μm on a Leica SM2000R freezing microtome. Amylo-Glo (TR-300-AG; Biosensis) staining was performed according to the manufacturer's instructions and as before (Spangenberg et al., 2019). Immunostained sections were mounted and coverslipped, then images were obtained using a Leica TCS SPE-II confocal microscope and LAS-X software. One 20× field-of-view (FOV) of the hippocampal CA1 was captured per mouse. Plaque number, area and intensity were determined using the surfaces module in Imaris v9.2.

2.7. In vivo calcium imaging data analysis

2.7.1. Firing rate maps and defining place cells—Data processing was performed with Matlab software using custom script (Sun et al., 2019). Miniscope recording data were frame-by-frame motion corrected and registered using a Non-Rigid method (NoRMCorre). Constrained non-negative matrix factorization for endoscopic recordings (CNMF-E) was used to extract calcium activity of individual neurons (Zhou et al., 2018). Spatial firing rate map was calculated using 1.5-cm-wide bins for OLM, 2-cm-wide bins for open field and 2.5-cm-wide bins for linear track test. The information content of a single neuron was defined using the following formula (Skaggs et al., 1993):

$$\text{Information score (bits per event)} = \sum_{i=1}^{N} Pi \frac{\lambda i}{\lambda} \ln \frac{\lambda i}{\lambda}.$$

where P_i represents the probability of the i-th bin's occupancy, λ_i represents the calcium event rate in the i-th bin and λ represents the overall average event rate. To define place cells, the event locations of each neuron were shuffled 500 times and the information content was recalculated for each shuffle. Then the value at 95% of the distribution of the shuffled information score was selected as the threshold of a significant measure.

2.7.2.   Analysis of open field data—The average calcium event rate (Hz) was determined from z-scored calcium events and thresholded at 2σ. Event amplitude (df/f) was calculated as (amplitude of an event - mean amplitude of all events)/mean amplitude of all events. The rate and amplitude of overall, mobile and immobile periods were analyzed. To analyze spatial encoding features, periods with animal speed lower than 1 cm/s were excluded, then (1) place field size; (2) information score; (3) sparsity; (4) spatial coherence; (5) inter-session rate map correlation; (6) within-session rate map correlation were calculated. For calculating place field area, inter-session and within session correlation, the rate maps were smoothed using Gaussian filter. Firing fields were located by the centers of rate map autocorrelation maps of neurons, and the place field size was calculated as the pixels of area with value higher than 50% of the autocorrelation peak. Information score is a function of the probability for the mice being at a location and the firing rate when the animal is being that location, therefore it represents a degree of spatial information that conveyed by the activity of the cell. Sparsity is a measure of the occupancy of the place field relative to the recording arena. Lower sparsity indicates more confined firing field. Spatial coherence is a measure of the spatial consistency of firing. It was calculated by replacing each pixel of the firing rate map matrix with the average of its eight neighbors, then was correlated to the original rate map. The coherence was represented by a Fisher's transform of the Pearson's R value: $Z = 0.5 \ln((1 + R)/(1 - R))$. Inter-session correlation was calculated by taking the Pearson correlation coefficient between the spatial firing rate maps of two sessions. Within session correlation was calculated by taking the Pearson correlation coefficient of rate maps between the 1st and 2nd halves of each session.

2.7.3.   Analysis of linear track data—For linear track data, inter-session correlation was calculated with the same method as described in open field analysis, and left-ward and right-ward directions were pooled to calculate rate maps. For encoding reliability within sessions, the behavior trajectory was separated into left-ward and right-ward directions, and trial-to-trial firing field was calculated in each direction. Firing field reliability was measured by within session trial-to-trial correlation and was computed for each cell via Pearson's correlation of the rate maps across trials.

2.7.4.   Analysis of OLM data—For OLM data, the ensemble activity surrounding each object location was evaluated by calculating the population vectors (Wilson and McNaughton, 1993). All rate maps were stacked into a 3-dimensional matrix with the spatial dimensions on the x and y axes and neurons on the z axis. The distribution of mean event rates along the z axis for each object location (within 3-bin-size distance surrounding the object) in training or testing session represents the population vector for that object. Then the correlation of population vectors between training and testing sessions was calculated for each object location.

2.8. Statistical analysis

Mouse behavior and pathology data were presented as mean ± SEM. We applied appropriate statistical tests per different experiment designs. For neural calcium activity and spatial encoding data, all neurons were pooled across animals, plotted by cumulative distribution and analyzed with Kolmogorov–Smirnov test (K–S test). To compare the average values between genotypes, data were presented by violin plot and analyzed with linear mixed effects model (lme) (Yu et al., 2022), using genotype as a fixed effect and mouse as a random effect. Other statistical methods including Student's *t*-test, Kruskal-Wallis and Dunn's post hoc test, 2-way ANOVA or Mann-Whitney *U* test were applied, where appropriate. Statistical analysis was conducted in the Matlab or Graphpad Prism 8 software. Alpha levels of p 0.05 were considered significant.

3. Results

3.1. Amyloid pathology is detected at 4 months of age in CA1 hippocampus in 5xFAD mice

We performed Amylo-Glo staining to measure amyloid-beta plaques in dorsal hippocampal CA1 brain sections from 4, 8 and 12-month-old 5xFAD and age matched WT control mice of a congenic C57BL/6strain background (Forner et al., 2021). As previously shown (Forner et al., 2021) and also in Fig. 1A, no plaques in WT mice are detected at any age (Fig. 1A). In contrast, amyloid plaques are clearly apparent at 4-months of age in 5xFAD mice and progressively increase with age. The number of amyloid plaques in CA1 area is significantly higher at 12 months compared with 4-month-old 5xFAD mice (Fig. 1B, 4-month: 17.44 ± 3.19 (average amyloid plaque number per field of view); 12-month: 38.0 ± 6.73. Kruskal-Wallis test, $p = 0.019$). The average plaque area and intensity do not differ among 4, 8, and 12 months 5xFAD mice. These results show early onset and the age-progressive increase in the amyloid pathology in 5xFAD mouse model.

3.2. 5xFAD mice develop OLM deficits at 8-month-old, accompanied by impaired neural discrimination of object-location combinations

To determine the time-course for development of memory deficits in 5xFAD model, we applied the object location memory test (OLM, Fig. 1C), and measured the differential in exploration time of the moved versus unmoved object in testing session by calculating the discrimination index (DI), where a positive DI indicates more exploration time on the moved object and memory of object locations. As shown in Fig. 1D, WT mice spend greater time exploring the moved object, quantified by a positive discrimination index (DI) score during the test session for all ages tested (4 to 14 months). Although amyloid plaques are present in 5xFAD mice at 4 months old, we do not observe OLM deficits at this age (4–5 m: WT: 0.174 ± 0.049; 5xFAD: 0.182 ± 0.039, $p = 0.91$). 5xFAD mice show impaired OLM starting at 8–10 months of age, as determined by their significantly decreased DI compared with age matched control (WT: 0.148 ± 0.038; 5xFAD: 0.038 ± 0.031. Student's *t*-test, t(16) = 2.172, $p = 0.045$), and the memory deficit persists in 14-month-old 5xFAD mice (WT: 0.206 ± 0.061; 5xFAD: 0.026 ± 0.048. Student's t-test, t(14) = 2.317, $p = 0.036$) (Fig. 1D). This shows that object location memory deficit occurs months later than amyloid pathology in 5xFAD mice.

During the behavioral test, we conducted in vivo calcium imaging of CA1 neuron populations using head-mounted miniscopes in freely moving mice expressing the genetically encoded calcium indicator GCaMP6 in excitatory neurons (Fig. 2A–C). The imaging method allows for simultaneous recording of large populations of CA1 neurons in behaving mice. To investigate the neural mechanisms underlying OLM deficits, we examined population activity patterns among CA1 neurons at locations associated with objects, and calculated population vector correlations between training and testing sessions for each object (Fig. 2D, E), to determine the degree to which discrimination of moved versus unmoved objects in CA1 neural activity patterns. In agreement with the finding that 5xFAD mice do not show OLM deficit at 4–5 months, 4–5-month-old 5xFAD mice also show comparable population vector correlation patterns as WT mice, which exhibit significantly higher population vector correlation for the unmoved object than the moved one (Fig. 2F) (WT: unmoved object: 0.201 ± 0.033, moved: 0.12 ± 0.021, $p = 0.0379$; 5xFAD: unmoved object: 0.172 ± 0.061, moved: 0.006 ± 0.035, $p = 0.0262$. Mann-Whitney U test), indicating relatively more stable CA1 representation for the unmoved object while different representation for the moved object. However, at 8–10-month when OLM deficit is observed in 5xFAD mice, the population vector correlation in 5xFAD mice is low for both unmoved and moved objects and no difference between objects, while WT mice still show higher correlation for the unmoved object than moved object (Fig. 2G) (WT: unmoved object: 0.387 ± 0.059, moved: 0.089 ± 0.02, $p = 0.0047$; 5xFAD: unmoved object: 0.159 ± 0.069, moved: 0.153 ± 0.085, $p = 0.71$. Mann-Whitney U test). This indicates that reliability in neural activity patterns at the site of the unmoved object is low in 8–10-month 5xFAD mice and that 5xFAD mice are unable to distinguish the moved and unmoved objects at population neuron levels, which coincides with memory deficits starting at 8–10 months in 5xFAD mice.

3.3.   5xFAD mice exhibit altered age-related trajectories in CA1 neural calcium activities

To determine whether physiological features of hippocampal CA1 neurons are altered in 5xFAD mice, we examined calcium event rates and amplitudes of hippocampal CA1 neurons as mice exploring circular and square shaped arenas (Fig. 3A). 5xFAD and WT mice showed comparable speed of open field exploration, indicating intact locomotion activity in 5xFAD mice and aged mice (Supplementary Fig. S5).

5xFAD mice show abnormalities in age-related trajectory of calcium event rates (Fig. 3B). At young ages (4–5 months) when preceding OLM deficits, the calcium event rates of population CA1 neurons in 5xFAD mice are significantly lower than those of WT mice (50%-cumulative values: WT 0.0454 Hz, 5xFAD 0.0379 Hz) (Fig. 3C). As age advancing, the population event rates for WT mice shift lower such that no difference in rates for WT and 5xFAD mice are observed at 14 months of age (Fig. 3C, 50%-cumulative values: WT 0.0246 Hz, 5xFAD 0.0258 Hz). As hippocampal activity is organized by theta oscillations in locomoting animals and into transient bursts in immobile animals (Buzáski et al., 1992), we next examined calcium event rates during mobile versus immobile states. At this level of detail, we find that hippocampal CA1 calcium event rates for mobile WT and 5xFAD mice differ minimally or not at all across development (Fig. 3D). Furthermore, 5xFAD mice exhibit significantly depressed event rates during immobile periods at all ages (Fig. 3E),

indicating that immobility calcium event rates presage memory deficits and that progressive differences in mobile versus immobile firing rates parallel deficits in spatial representation (as detailed below).

Abnormal age-related trajectories in 5xFAD mice are also observed for calcium event amplitudes with 5xFAD mice showing higher average amplitudes, relative to WT, at early stages (Fig. 4A, 4–5 months, 50%-cumulative values: WT 14.97 df/f, 5xFAD 16.11 df/f) and substantially lower amplitudes at 14 months of age (Fig. 4A. 50%-cumulative values at 14-month: WT 24.39 df/f, 5xFAD 16.52 df/f). The differences between WT and 5xFAD mice are a consequence of the progressive shift of event amplitudes in WT mice to higher values, while 5xFAD amplitudes show little change with age advancing. And this trend is similar in both mobile and immobile periods during open field exploration (Fig. 4B,C). We also observed similar abnormalities of calcium activity in 5xFAD mice in square arena exploration (Supplementary Fig. S6). These data indicate that calcium event rates and amplitude distributions in 5xFAD are abnormally stable across the age range of 4–14 months relative to WT distributions which shift across the lifespan, and altered hippocampal CA1 calcium activities in 5xFAD mice appear at early stage preceding OLM deficit.

3.4. Degraded spatial tuning of CA1 neurons in open field precedes OLM deficits in 5xFAD mice

Based on the altered age-related trajectory in CA1 calcium activity in 5xFAD mice, we then asked whether spatial representation in CA1 neuron populations is altered in 5xFAD mice during open field exploration and, if so, when such alterations are observed. CA1 neurons in both WT and 5xFAD mice exhibit spatially tuned activity in open field (Fig. 5A), but significant alterations in tuning of CA1 neurons in 5xFAD mice reveals degraded and unreliable tuning to environment location. By deriving the spatial autocorrelation rate maps, we find that the place fields are smaller in 5xFAD mice (Fig. 5B) and that this difference emerges as early as 4–5 months of age (50%-cumulative values at 4–5-month: WT 65 pixels, 5xFAD 56.5 pixels). Accordingly, 5xFAD mice show higher spatial information score (bits per event) at all ages compared with WT (Fig. 5C, 50%-cumulative values: 4–5-m: WT 2.75, 5xFAD 2.89; 8–10-m: WT 3.03, 5xFAD 3.31; 14-m: WT 2.01, 5xFAD 3.12). Information score has previously been used as a metric to judge the place specificity of spiking activity in rate maps (Skaggs et al., 1993; Hargreaves et al., 2005). However, this measure is mathematically sensitive to only the distribution of calcium event rates across spatial bins of an environment, yielding higher values when only a small proportion of spatial bins are associated with higher activity rates and a much larger proportion is associated with low or zero activity rates. Thus, we asked whether the higher information score in 5xFAD mice can be explained by several complementary metrics for spatial tuning that can put the spatial information scores in context.

First, we examined the metric sparsity which is sensitive to the proportion of environmental locations associated with higher activity rates, finding lower values in 5xFAD mice at all ages tested (Fig. 5D, 50%-cumulative values: 4–5-m: WT 0.128, 5xFAD 0.111; 8–10-m: WT 0.105, 5xFAD 0.089; 14-m: WT 0.208, 5xFAD 0.098). This measure is consistent with our measured higher information score in 5xFAD mice. We also assessed coherence, a

measure that addresses the extent to which spatial bins with higher firing rates are clustered in environmental space. While a slight increase in coherence of population neuron level is found in 4–5-month-old 5xFAD mice, this difference reverses greatly by 8–10 months and large reductions in coherence are found in older 14 months 5xFAD mice relative to WT control mice (Fig. 5E, 50%-cumulative values: 4–5-m: WT 0.208, 5xFAD 0.222; 8–10-m: WT 0.222, 5xFAD 0.19; 14-m: WT 0.253, 5xFAD 0.158). Finally, we find reduced inter-session correlation in the activity rate maps for 5xFAD mice aged 8 months and above across 4 days of exploration in the same environment (Fig. 5F, 50%-cumulative values: 8–10-m: WT 0.492, 5xFAD 0.354; 14-m: WT 0.451, 5xFAD 0.207), and reduced correlation of rate maps for different periods within the same exploration session starting at 4–5-month-old 5xFAD mice (Fig. 5G, 50%-cumulative values: 4–5-m: WT 0.551, 5xFAD 0.494; 8–10-m: WT 0.553, 5xFAD 0.487; 14-m: WT 0.425, 5xFAD 0.372). We also examined the sex difference of encoding stability and found that CA1 cells in female 5xFAD mice show significantly lower inter-session rate map correlation than those of male mice in open field experiments at all ages (Supplementary Fig. S3B), indicating more impaired encoding stability in female AD mice. This is consistent with the more severe amyloid pathology in female 5xFAD mice (Forner et al., 2021). In the square open field arena, we also observed similar degraded tuning in 5xFAD mice as in the circle arena (Supplementary Fig. S7). The combined data show that dramatic impairments of spatial encoding appear at 8–10-month when animals show OLM, however, some aspects of degraded and unstable tuning is detectable at 4–5-month which precedes OLM deficit.

3.5. Unreliable spatial encoding during linear track test starting at 4–5 months precedes OLM deficit in 5xFAD mice

The instability in spatial tuning in open field environments for 5xFAD mice, particularly obvious at 8–10 months and older, suggests a possible explanation for the OLM deficits that emerge at 8–10 months in 5xFAD mice. Still, instability across exploration sessions or across different time periods within the same exploration session might reflect variation in the specific trajectories taken across different exploration time periods (Markus et al., 1995).

To more directly address the degree of instability in spatial tuning of CA1 neurons in 5xFAD mice, we also examined firing fields stability along a straight track when animals shuttle back and forth between the track's end locations (Fig. 6A, B). Even in 4–5-month 5xFAD mice, small but significant reductions in the correlation of rate maps are observed across sessions of the same track orientations (Fig. 6C. 50%-cumulative values at 4–5 m: WT 0.479, 5xFAD 0.40. Fig. 6D, 50%-cumulative values at 4–5 m: WT 0.552, 5xFAD 0.468). At 14 months of age, the instability in 5xFAD mice are much greater, as shown by much lower rate map correlations across sessions (Fig. 6C, 50%-cumulative values at 14 m: WT 0.528, 5xFAD 0.297. Fig. 6D, 50%-cumulative values at 14 m: WT 0.372, 5xFAD 0.13). We also examined the sex difference and found that CA1 cells in female 5xFAD mice show lower inter-session rate map correlation than male CA1 cells in at 4–5-m- and 8–10-m-old (Supplementary Fig. S4). These results indicate that WT mice show stable encoding across ages, while 5xFAD mice exhibit impaired encoding stability in the same linear track starting at as early as 4–5-month-old.

In comparing activity patterns with different orientations to the recording room space, both WT and 5xFAD mice show changes of firing rate maps when orientation changes at 4–5 and 8–10 months, as revealed by a low rate map correlation between the two orientations (Fig. 7A). However, we were surprised to find that aged (14 months) WT animals exhibit generalization in their spatial firing patterns. In contrast, 5xFAD mice show no such generalization pattern with different track orientations (Fig. 7A, 14 months, 50%-cumulative values of rate map correlation: WT 0.527, 5xFAD 0.153). Examination of within-session, trial-to-trial correlation of activity fields of CA1 neurons reveals much larger deficits in 5xFAD mice that are observable even at 4–5-month (Fig. 7B). Whereas CA1 neurons of WT animals exhibit relatively high trial-to-trial reliability in activity fields within session, CA1 neurons in 5xFAD mice do not (Fig. 7C, 50%-cumulative values: 4–5-m: WT 0.549, 5xFAD 0.483; 8–10-m: WT 0.464, 5xFAD 0.411; 14-m: WT: 0.609, 5xFAD 0.424). Thus, at early ages, the reduced activity rates of CA1 neurons in 5xFAD mice (Fig. 3) appear to reflect the absence of reliable location-specific coding across trials even though the animals traverse such spaces with a consistent heading that should maximize similarity across trials. Such trial-to-trial impairments in reliability of spatial tuning can be expected to depress co-activity for neurons with spatial tuning for the same location and, in turn, this can be expected to negatively impact memory formation.

3.6. Suppressed CA1 neuron calcium activity and unreliable spatial encoding at early stage predict OLM deficit at older age

The above data indicate abnormal circuit activity in 5xFAD mice at 4–5-month-old, including suppressed calcium event rate, decreased within-session correlation in open field, higher information score, decreased inter-session and trial-to-trial correlations in linear track, we then asked if animals showing these abnormal features at early stage exhibit impaired OLM at 8–10-month-old. We analyzed the correlation between neuron activity or encoding features at 4–5-month of individual animals with their OLM performance at 8–10-month. The result shows that suppressed calcium event rate and lower trial-to-trial stability in linear track at 4–5-month significantly correlated with lower DI in OLM test (Fig. 8A, D), lower within-session stability in open field and lower inter-session stability in linear track show a slight trend of correlation with lower DI (Fig. 8B, E), while information score does not show correlation with OLM performance (Fig. 8C). This result indicates that suppressed CA1 neuronal activity and unreliable spatial encoding at early stage predict OLM deficits at older age.

4. Discussion

We investigated how object location memory deficits progress in 5xFAD versus WT mice and how such age-related deficits parallel alterations in hippocampal CA1 network dynamics. Building on our earlier imaging work (Lin et al., 2022), this present study is the first extensive investigation that applies longitudinally repeated, task-related calcium imaging in a single cohort of mice. We find that WT mice maintain intact object location memory and stable spatial encoding up to 14 months old. 5xFAD mice show amyloid pathology, depressed neuronal calcium rates during immobile states and unreliable spatial encoding at as early as 4 months old. These circuit degradations precede OLM deficits

and degradation of CA1 representation of object-location pairings that can be detected at 8–10 months of age. Thus, our work advances conceptualizations that dysfunction in hippocampal networks presages the emergence of behavioral memory deficits in AD. Our examination of reliability in spatial tuning and tuning to object-locations provide insight into how failures in neuron ensemble level discrimination of different object occupied locations can be related with OLM deficits. Furthermore, animals showing suppressed calcium event rate and unreliable spatial encoding at 4–5-month exhibit worse memory in OLM test at 8–10-month, indicating that measures of overall hippocampal activity during immobility and reliability in hippocampal encoding in spatial environments could be highly sensitive to early disease detection.

Previous studies report that the 5xFAD model develops amyloid deposition at 2–4 months of age (Oakley et al., 2006; Caccavano et al., 2020; Forner et al., 2021). Deficits in synaptic transmission and long-term potentiation have been observed at 4 to 6 months old (Kimura and Ohno, 2009; Crouzin et al., 2013; Forner et al., 2021). Although slight impairments of spatial memory or hippocampus-independent memory can be detected at 3 to 4-month-old in 5xFAD mice (Kimura and Ohno, 2009; Girard et al., 2014; Caccavano et al., 2020), more obvious memory deficits appear at later ages (after 4–6-month) (Oakley et al., 2006; Girard et al., 2014; Martorell et al., 2019). Our findings in OLM test extend these studies that neuropathological features do not lead immediately to memory deficits, instead, alterations in CA1 network activity parallel pathology and emerge at early ages in 5xFAD mice with intact object memory.

Our study indicates that progressive degradation in spatial representation and, eventually, impaired tuning of neural activity to object-location pairings at 8–10-month, appear to be related with OLM deficits. CA1 neuronal representations of object-location pairings is evaluated by calculating the population vector correlations at the sites of moved and unmoved objects for training versus testing sessions of OLM test. In WT mice, a higher population vector correlation for the unmoved object than the moved object indicates a relatively more stable encoding at the location of unmoved object and discrimination between objects. However, in 8–10-month-old 5xFAD mice with OLM deficit, the population vector correlations for both objects are similarly low, indicating impaired CA1 representation of object-location pairings and lack of discrimination of objects at neuron level. The latter effect is perhaps explained by the lack of reliability in CA1 encoding which is detected during open-field and track-running behavior. Given the dependence of OLM on intact hippocampal function (Assini et al., 2009; Barker and Warburton, 2011), these data indicate, for the first time, that there is a close connection between impaired hippocampal tuning to object locations and the presence of OLM deficits.

Our longitudinal imaging indicates that CA1 neurons in WT mice follow an age-related pattern for calcium activity rates which gradually decrease with age advancing relative to 5xFAD mice whose CA1 neuron populations are abnormally static in their mean activity rates. As a result, 5xFAD mean rates overall are abnormally low at early ages and statistically normal in aged animals. Hippocampal activity is organized by theta oscillations in locomoting animals and into slower, more irregular field potential activity punctuated by sharp wave ripple (SWR) events during slow wave sleep and wakeful immobility, which

plays a causal role in memory consolidation (Buzáski et al., 1992; Girardeau et al., 2009). A different picture emerges when mean firing rates are split between mobile versus immobile locomotion periods. In our study, we find that hippocampal CA1 calcium event rates for mobile WT and 5xFAD mice differ minimally or not at all across development (Fig. 3C), but that 5xFAD mice show lower calcium rates significantly in the immobile periods of open field exploration at early ages (4–5-month, Fig. 3D), which persists and are exacerbated in later stages of development when memory deficits appear. Earlier studies report both increased and decreased neuronal activity depending on models, such as hyperexcitability in amyloid models (Busche et al., 2012; Sompol et al., 2017), hypoactivity in Tau models (Cheng and Ji, 2013; Ciupek et al., 2015; Booth et al., 2016; Fu et al., 2017; Mably et al., 2017), and slightly decreased activity in 5xFAD model (Prince et al., 2021). Also, the hippocampal activity is experience dependent (O'Neill et al., 2008; Dupret et al., 2010), and place cells in APP model mice show lower activity than WT in a familiar environment (Zhao et al., 2014), probably due to impaired reactivation when revisiting the environment. Our result of depressed CA1 calcium activity in 5xFAD mice appears to reflect the depressed co-activity for neurons with spatial tuning for the same location. Together with previous report of abnormal SWR activity in 5xFAD model (Iaccarino et al., 2016), our results suggest that altered activity during immobility and unreliable spatial encoding probably underlies memory deficits of AD. Our results also suggest that measuring the circuit activity during resting versus moving periods is a potential method to detect AD at early stages.

Spatially tuned CA1 "place cells" store and recall the spatial maps for environments and this is considered as the foundation of spatial memory. Disrupted place cell function has been reported in several transgenic AD models using electrical tetrode recordings at discreet time points (Cacucci et al., 2008; Cheng and Ji, 2013; Mably et al., 2017; Galloway et al., 2018; Jun et al., 2020; Prince et al., 2021). We have recently used miniscope imaging to examine hippocampal calcium activities in a triple-transgenic AD model (3xTg-AD) that presents both amyloid plaque and neurofibrillary pathological features along with age-related behavioral deficits (Lin et al., 2022). We identify age-dependent differences of calcium activity and less place specificity for spatial representation in 3xTg-AD mice. A widely used feature for spatial encoding is information score, which attempts to measure the degree of spatial information that is conveyed by neuron activity. In our current study, 5xFAD mice show higher information scores in open field tests at all ages. Since the information score is a function of firing frequency and the probability of occupancy of bins in the arena, we also calculated sparsity, which measures the occupancy of the firing field relative to the arena. 5xFAD mice exhibit lower sparsity and smaller place field size at all ages tested (Fig. 5B, D), generating a higher information score. Although many studies indicate that a higher information score measures better spatial specificity (Cacucci et al., 2008; Henriksen et al., 2010; Mably et al., 2017), the mathematical design of this metric allows for spatially distributed firing to yield equal or higher information scores than is seen for spatially ordered representation. This appears to be the case in 5xFAD mice since CA1 neuron calcium activity from 5xFAD mice has significantly lower coherence in open field starting from the age of 8–10 months (Fig. 5E), which better reflects the extent of spatial continuity of activity. Furthermore, by comparing the spatial encoding reliability within sessions (Fig. 5G), CA1 neurons in 5xFAD mice show unreliable spatial encoding

at as early as 4–5-month. This indicates that the information score itself cannot in all cases be considered to reflect stronger spatial representation and must be put into the context of other measures looking at spatial coherence and reliability. Notably, spatial coherence and reliability likely better reflect the extent to which neurons with similar tuning fields exhibit the co-activity patterns, which are key to synaptic potentiation and memory formation (Muller and Kubie, 1989; Bliss and Collingridge, 1993).

The function of "remapping" supports the discrimination of different environments (Leutgeb et al., 2005; Jun et al., 2020; Schuette et al., 2020). Indeed, CA1 neurons in 4–5- and 8–10-month-old WT mice show global remapping on linear track when the track rotates 90 degrees relative to the environments (Fig. 7A). 5xFAD mice also show different CA1 population activity patterns between different track orientations. To test whether this finding reflected true shifts in mapping or, instead, noisier spatial tuning, we analyzed the encoding reliability across trials within sessions of track running. CA1 neurons in WT mice show stable trial-to-trial firing field in both the initial and rotated track orientations at all ages (Fig. 7B,C). On the contrary, CA1 neurons of 5xFAD mice show significantly decreased within session trial-to-trial rate map correlation starting at the age of 4–5 months, indicating disrupted encoding reliability starting in young AD mice. Thus, the distinct rate maps observed in different track orientations in 5xFAD mice appear to be a consequence of unreliable encoding across trials, rather than a real "remapping". Interestingly, we observed diminished remapping in older WT mice, revealed by more generalized rate maps between different track orientations (Fig. 7A, 14 months). The spatial representation of hippocampus on linear track is flexible with track length and largely shaped by the training experience across trials (Kjelstrup et al., 2008; Dombeck et al., 2010; Navratilova et al., 2012; Ziv et al., 2013; Sun et al., 2020). Since in our longitudinal research, the same cohort of mice was repeatedly tested on linear track, further studies are needed to determine how the training experience affects generalization in older animals.

Our study demonstrates that amyloid accumulation and circuit level deficits precede age-related OLM deficits in 5xFAD mice, recapitulating a critical feature of human AD. Abnormalities in the fundamental features (rate and amplitude) of CA1 neuronal calcium activity and unreliable spatial encoding in CA1 neurons are detected in 5xFAD mice at as early as 4–5-months of age. Progressive degradation of spatial encoding and impaired representation of object locations are accompanied by OLM deficits at 8–10-months of age. Furthermore, suppressed calcium event rate and lower trial-to-trial stability in linear track at 4–5-month are significantly correlated with lower DI in OLM test at 8–10-month, indicating circuit deficits measured at early stage predict OLM deficits. While we focus on the CA1 area in this study, we plan to study the extensive hippocampal formation networks including the input and output areas of CA1 in AD mouse models. We will also plan to expand our studies to include other AD models such as novel mouse models of late-onset Alzheimer's disease (LOAD) from the Model-AD Consortium supported by the US National Institute on Aging. Overall, our results suggest that measurements of reliability of hippocampal spatial representation and baseline firing rates during active moving versus immobility could provide early opportunities for AD detection.

Supplementary Material

Refer to Web version on PubMed Central for supplementary material.

Funding sources

Data availability

Data will be made available on request. Data available on reasonable request from the corresponding author.

Abbreviation:

AD	Alzheimer's disease
CNMF-E	Constrained non-negative matrix factorization for endoscopic recordings
DI	discrimination index
K-S test	Kolmogorov–Smirnov test
lme	linear mixed effects model
OLM	object location memory
SWRs	sharp wave ripples
WT	wild type

References

Assini FL, Duzzioni M, Takahashi RN, 2009. Object location memory in mice: pharmacological validation and further evidence of hippocampal CA1 participation. Behav. Brain Res. 204, 206–211. [PubMed: 19523494]

Barker GR, Warburton EC, 2011. When is the hippocampus involved in recognition memory? J. Neurosci. 31, 10721–10731. [PubMed: 21775615]

Barnes CA, Suster MS, Shen J, McNaughton BL, 1997. Multistability of cognitive maps in the hippocampus of old rats. Nature 388, 272–275. [PubMed: 9230435]

Barrett RM, Malvaez M, Kramar E, Matheos DP, Arrizon A, Cabrera SM, Lynch G, Greene RW, Wood MA, 2011. Hippocampal focal knockout of CBP affects specific histone modifications, long-term potentiation, and long-term memory. Neuropsychopharmacology 36, 1545–1556. [PubMed: 21508930]

Bliss TVP, Collingridge GL, 1993. A synaptic model of memory: long-term potentiation in the hippocampus. Nature 361, 31–39. [PubMed: 8421494]

Booth CA, Witton J, Nowacki J, Tsaneva-Atanasova K, Jones MW, Randall AD, Brown JT, 2016. Altered intrinsic pyramidal neuron properties and pathway-specific synaptic dysfunction underlie aberrant hippocampal network function in a mouse model of Tauopathy. J. Neurosci. 36, 350–363. [PubMed: 26758828]

Busche MA, Chen X, Henning HA, Reichwald J, Staufenbiel M, Sakmann B, Konnerth A, 2012. Critical role of soluble amyloid-beta for early hippocampal hyperactivity in a mouse model of Alzheimer's disease. Proc. Natl. Acad. Sci. U. S. A. 109, 8740–8745. [PubMed: 22592800]

Buzáski G, Horváth Z, Urioste R, Hetke J, Wise K, 1992. High-frequency network oscillation in the hippocampus. Science 256, 1025–1027. [PubMed: 1589772]

Caccavano A, Bozzelli PL, Forcelli PA, Pak DTS, Wu J-Y, Conant K, Vicini S, 2020. Inhibitory parvalbumin basket cell activity is selectively reduced during hippocampal sharp wave ripples in a mouse model of familial Alzheimer's disease. J. Neurosci. 40, 5116–5136. [PubMed: 32439703]

Cacucci F, Yi M, Wills TJ, Chapman P, O'Keefe J, 2008. Place cell firing correlates with memory deficits and amyloid plaque burden in Tg2576 Alzheimer mouse model. Proc. Natl. Acad. Sci. 105, 7863–7868. [PubMed: 18505838]

Canter RG, Penney J, Tsai L-H, 2016. The road to restoring neural circuits for the treatment of Alzheimer's disease. Nature 539, 187–196. [PubMed: 27830780]

Cheng J, Ji D, 2013. Rigid firing sequences undermine spatial memory codes in a neurodegenerative mouse model. Elife 2, e00647. [PubMed: 23805379]

Ciupek SM, Cheng J, Ali YO, Lu HC, Ji D, 2015. Progressive functional impairments of hippocampal neurons in a Tauopathy mouse model. J. Neurosci. 35, 8118–8131. [PubMed: 26019329]

Crouzin N, Baranger K, Cavalier M, Marchalant Y, Cohen-Solal C, Roman FS, Khrestchatisky M, Rivera S, Feron F, Vignes M, 2013. Area-specific alterations of synaptic plasticity in the 5XFAD mouse model of Alzheimer's disease: dissociation between somatosensory cortex and hippocampus. PLoS One 8, e74667. [PubMed: 24069328]

Dautricourt S, Flores R, Landeau B, Poisnel G, Vanhoutte M, Delcroix N, Eustache F, Vivien D, Sayette V, Chételat G, 2021. Longitudinal changes in hippocampal network connectivity in Alzheimer's disease. Ann. Neurol. 90, 391–406. [PubMed: 34279043]

Dombeck DA, Harvey CD, Tian L, Looger LL, Tank DW, 2010. Functional imaging of hippocampal place cells at cellular resolution during virtual navigation. Nat. Neurosci. 13, 1433–1440. [PubMed: 20890294]

Dupret D, O'Neill J, Pleydell-Bouverie B, Csicsvari J, 2010. The reorganization and reactivation of hippocampal maps predict spatial memory performance. Nat. Neurosci. 13, 995–1002. [PubMed: 20639874]

Forner S, et al. , 2021. Systematic phenotyping and characterization of the 5xFAD mouse model of Alzheimer's disease. Sci. Data 8, 270. [PubMed: 34654824]

Fu H, Rodriguez GA, Herman M, Emrani S, Nahmani E, Barrett G, Figueroa HY, Goldberg E, Hussaini SA, Duff KE, 2017. Tau pathology induces excitatory neuron loss, grid cell dysfunction, and spatial memory deficits reminiscent of early Alzheimer's disease. Neuron 93, 533–541.e535. [PubMed: 28111080]

Galloway CR, Ravipati K, Singh S, Lebois EP, Cohen RM, Levey AI, Manns JR, 2018. Hippocampal place cell dysfunction and the effects of muscarinic M1 receptor agonism in a rat model of Alzheimer's disease. Hippocampus 28, 568–585. [PubMed: 29742799]

Girard SD, Jacquet M, Baranger K, Migliorati M, Escoffier G, Bernard A, Khrestchatisky M, Féron F, Rivera S, Roman FS, Marchetti E, 2014. Onset of hippocampus-dependent memory impairments in 5XFAD transgenic mouse model of Alzheimer's disease. Hippocampus 24, 762–772. [PubMed: 24596271]

Girardeau G, Benchenane K, Wiener SI, Buzsáki G, Zugaro MB, 2009. Selective suppression of hippocampal ripples impairs spatial memory. Nat. Neurosci. 12, 1222–1223. [PubMed: 19749750]

Hargreaves EL, Rao G, Lee I, Knierim JJ, 2005. Major dissociation between medial and lateral entorhinal input to dorsal hippocampus. Science 308, 1792–1794. [PubMed: 15961670]

Harris SS, Wolf F, De Strooper B, Busche MA, 2020. Tipping the scales: peptide-dependent dysregulation of neural circuit dynamics in Alzheimer's disease. Neuron 107, 417–435. [PubMed: 32579881]

Henriksen EJ, Colgin LL, Barnes CA, Witter MP, Moser M-B, Moser EI, 2010. Spatial representation along the proximodistal axis of CA1. Neuron 68, 127–137. [PubMed: 20920796]

Iaccarino HF, Singer AC, Martorell AJ, Rudenko A, Gao F, Gillingham TZ, Mathys H, Seo J, Kritskiy O, Abdurrob F, Adaikkan C, Canter RG, Rueda R, Brown EN, Boyden ES, Tsai L-H, 2016.

Gamma frequency entrainment attenuates amyloid load and modifies microglia. Nature 540, 230–235. [PubMed: 27929004]

Jack CR, Knopman DS, Jagust WJ, Petersen RC, Weiner MW, Aisen PS, Shaw LM, Vemuri P, Wiste HJ, Weigand SD, Lesnick TG, Pankratz VS, Donohue MC, Trojanowski JQ, 2013. Tracking pathophysiological processes in Alzheimer's disease: an updated hypothetical model of dynamic biomarkers. Lancet Neurol. 12, 207–216. [PubMed: 23332364]

Jun H, Bramian A, Soma S, Saito T, Saido TC, Igarashi KM, 2020. Disrupted place cell remapping and impaired grid cells in a knockin model of Alzheimer's disease. Neuron 107, 1095–1112.e1096. [PubMed: 32697942]

Kentros C, Hargreaves E, Hawkins RD, Kandel ER, Shapiro M, Muller RV, 1998. Abolition of long-term stability of new hippocampal place cell maps by NMDA receptor blockade. Science 280, 2121–2126. [PubMed: 9641919]

Kimura R, Ohno M, 2009. Impairments in remote memory stabilization precede hippocampal synaptic and cognitive failures in 5XFAD Alzheimer mouse model. Neurobiol. Dis. 33, 229–235. [PubMed: 19026746]

Kjelstrup KB, Solstad T, Brun VH, Hafting T, Leutgeb S, Witter MP, Moser EI, Moser MB, 2008. Finite scale of spatial representation in the hippocampus. Science 321, 140–143. [PubMed: 18599792]

Leutgeb S, Leutgeb JK, Barnes CA, Moser EI, McNaughton BL, Moser MB, 2005. Independent codes for spatial and episodic memory in hippocampal neuronal ensembles. Science 309, 619–623. [PubMed: 16040709]

Lin X, Chen L, Baglietto-Vargas D, Kamalipour P, Ye Q, LaFerla FM, Nitz DA, Holmes TC, Xu X, 2022. Spatial coding defects of hippocampal neural ensemble calcium activities in the triple-transgenic Alzheimer's disease mouse model. Neurobiol. Dis. 162, 105562. [PubMed: 34838667]

Mably AJ, Gereke BJ, Jones DT, Colgin LL, 2017. Impairments in spatial representations and rhythmic coordination of place cells in the 3xTg mouse model of Alzheimer's disease. Hippocampus 27, 378–392. [PubMed: 28032686]

Markus EJ, Qin YL, Leonard B, Skaggs WE, McNaughton BL, Barnes CA, 1995. Interactions between location and task affect the spatial and directional firing of hippocampal neurons. J. Neurosci. 15, 7079–7094. [PubMed: 7472463]

Martorell AJ, Paulson AL, Suk H-J, Abdurrob F, Drummond GT, Guan W, Young JZ, Kim DN-W, Kritskiy O, Barker SJ, Mangena V, Prince SM, Brown EN, Chung K, Boyden ES, Singer AC, Tsai L-H, 2019. Multi-sensory gamma stimulation ameliorates Alzheimer's-associated pathology and improves cognition. Cell 177, 256–271.e222. [PubMed: 30879788]

McHugh TJ, Blum KI, Tsien JZ, Tonegawa S, Wilson MA, 1996. Impaired hippocampal representation of space in CA1-specific NMDAR1 knockout mice. Cell 87, 1339–1349. [PubMed: 8980239]

Muffato V, Hilton C, Meneghetti C, De Beni R, Wiener JM, 2019. Evidence for age-related deficits in object-location binding during place recognition. Hippocampus 29, 971–979. [PubMed: 31070289]

Muller RU, Kubie JL, 1989. The firing of hippocampal place cells predicts the future position of freely moving rats. J. Neurosci. 9, 4101–4110. [PubMed: 2592993]

Muller RU, Kubie JL, Ranck JB, 1987. Spatial firing patterns of hippocampal complex-spike cells in a fixed environment. J. Neurosci. 7, 1935–1950. [PubMed: 3612225]

Murai T, Okuda S, Tanaka T, Ohta H, 2007. Characteristics of object location memory in mice: behavioral and pharmacological studies. Physiol. Behav. 90, 116–124. [PubMed: 17049363]

Navratilova Z, Hoang LT, Schwindel CD, Tatsuno M, McNaughton BL, 2012. Experience-dependent firing rate remapping generates directional selectivity in hippocampal place cells. Front. Neural Circ. 6.

Oakley H, Cole SL, Logan S, Maus E, Shao P, Craft J, Guillozet-Bongaarts A, Ohno M, Disterhoft J, Van Eldik L, Berry R, Vassar R, 2006. Intraneuronal beta-amyloid aggregates, neurodegeneration, and neuron loss in transgenic mice with five familial Alzheimer's disease mutations: potential factors in amyloid plaque formation. J. Neurosci. 26, 10129–10140. [PubMed: 17021169]

O'Keefe J, Dostrovsky J, 1971. The hippocampus as a spatial map. Preliminary evidence from unit activity in the freely-moving rat. Brain Res. 34, 171–175. [PubMed: 5124915]

O'Neill J, Senior TJ, Allen K, Huxter JR, Csicsvari J, 2008. Reactivation of experience-dependent cell assembly patterns in the hippocampus. Nat. Neurosci. 11, 209–215. [PubMed: 18193040]

Prince SM, Paulson AL, Jeong N, Zhang L, Amigues S, Singer AC, 2021. Alzheimer's pathology causes impaired inhibitory connections and reactivation of spatial codes during spatial navigation. Cell Rep. 35, 109008. [PubMed: 33882308]

Schuette PJ, Reis FMCV, Maesta-Pereira S, Chakerian M, Torossian A, Blair GJ, Wang W, Blair HT, Fanselow MS, Kao JC, Adhikari A, 2020. Long-term characterization of hippocampal remapping during contextual fear acquisition and extinction. J. Neurosci. 40, 8329–8342. [PubMed: 32958567]

Shinohara Y, Hosoya A, Yamasaki N, Ahmed H, Hattori S, Eguchi M, Yamaguchi S, Miyakawa T, Hirase H, Shigemoto R, 2012. Right-hemispheric dominance of spatial memory in split-brain mice. Hippocampus 22, 117–121. [PubMed: 21069782]

Skaggs WE, McNaughton BL, Gothard KM, Markus EJ, 1993. An information-theoretic approach to deciphering the hippocampal code. In: Hanson SJ, Cowan JD, Giles CL (Eds.), Advances in Neural Processing Systems, vol. 5. Morgan Kaufmann, pp. 1030–1037.

Sompol P, Furman JL, Pleiss MM, Kraner SD, Artiushin IA, Batten SR, Quintero JE, Simmerman LA, Beckett TL, Lovell MA, Murphy MP, Gerhardt GA, Norris CM, 2017. Calcineurin/NFAT signaling in activated astrocytes drives network hyperexcitability in Aβ-bearing mice. J. Neurosci. 37, 6132–6148. [PubMed: 28559377]

Spangenberg E, et al. , 2019. Sustained microglial depletion with CSF1R inhibitor impairs parenchymal plaque development in an Alzheimer's disease model. Nat. Commun. 10, 3758. [PubMed: 31434879]

Sun Y, Jin S, Lin X, Chen L, Qiao X, Jiang L, Zhou P, Johnston KG, Golshani P, Nie Q, Holmes TC, Nitz DA, Xu X, 2019. CA1-projecting subiculum neurons facilitate object–place learning. Nat. Neurosci. 22, 1857–1870. [PubMed: 31548723]

Sun C, Yang W, Martin J, Tonegawa S, 2020. Hippocampal neurons represent events as transferable units of experience. Nat. Neurosci. 23, 651–663. [PubMed: 32251386]

Veitch DP, Weiner MW, Aisen PS, Beckett LA, Cairns NJ, Green RC, Harvey D, Jack CR, Jagust W, Morris JC, Petersen RC, Saykin AJ, Shaw LM, Toga AW, Trojanowski JQ, 2018. Understanding disease progression and improving Alzheimer's disease clinical trials: recent highlights from the Alzheimer's disease neuroimaging initiative. Alzheimers Dement. 15, 106–152. [PubMed: 30321505]

Wilson MA, McNaughton BL, 1993. Dynamics of the hippocampal ensemble code for space. Science 261, 1055–1058. [PubMed: 8351520]

Yu Z, Guindani M, Grieco SF, Chen L, Holmes TC, Xu X, 2022. Beyond t test and ANOVA: applications of mixed-effects models for more rigorous statistical analysis in neuroscience research. Neuron 110, 21–35. [PubMed: 34784504]

Zhao R, Fowler SW, Chiang AC, Ji D, Jankowsky JL, 2014. Impairments in experience-dependent scaling and stability of hippocampal place fields limit spatial learning in a mouse model of Alzheimer's disease. Hippocampus 24, 963–978. [PubMed: 24752989]

Zhou P, Resendez SL, Rodriguez-Romaguera J, Jimenez JC, Neufeld SQ, Giovannucci A, Friedrich J, Pnevmatikakis EA, Stuber GD, Hen R, Kheirbek MA, Sabatini BL, Kass RE, Paninski L, 2018. Efficient and accurate extraction of in vivo calcium signals from microendoscopic video data. eLife 7.

Ziv Y, Burns LD, Cocker ED, Hamel EO, Ghosh KK, Kitch LJ, Gamal AE, Schnitzer MJ, 2013. Long-term dynamics of CA1 hippocampal place codes. Nat. Neurosci. 16, 264–266. [PubMed: 23396101]

Zokaei N, Sillence A, Kienast A, Drew D, Plant O, Slavkova E, Manohar SG, Husain M, 2020. Different patterns of short-term memory deficit in Alzheimer's disease, Parkinson's disease and subjective cognitive impairment. Cortex 132, 41–50. [PubMed: 32919108]
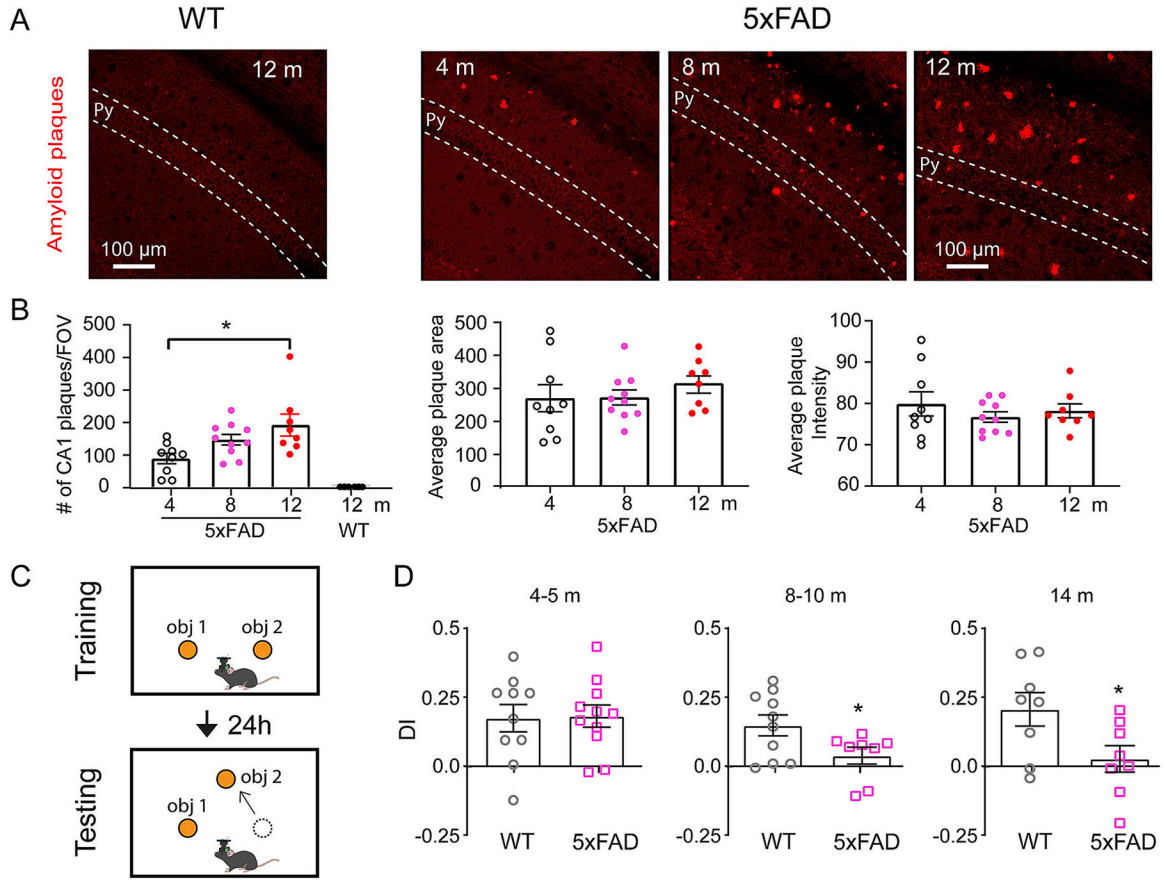
Fig. 1.

The appearance of amyloid pathology precedes object location memory behavioral deficits that occur at 8 months of age in 5xFAD mice. A. Representative histology images show no amyloid pathology detected in WT mouse hippocampal CA1, and age-dependent amyloid pathology in CA1 area of 5xFAD mice. Py, pyramidal cell layer. B. From left to right: quantification of the number of plaques in CA1 area, average plaque area and average plaque intensity. 5xFAD mice show significantly higher number of plaques at 12 months compared with 4 months (Kruskal-Wallis test, $p = 0.0174$. 4-m vs 12-m, post hoc comparison, $p = 0.019$). 5xFAD mice: $n = 9$ for 4-month, 10 for 8-month and 8 for 12-month. WT $n = 8$. C. Schematic of OLM test. Mice were exposed to two identical objects in the training session and were tested after 24 h with one object moved to a new location. The discrimination index (DI) during testing session was calculated. D. 5xFAD mice show decreased DI starting from 8 to 10 months old. 4–5 months: student's t test, $p = 0.91$. WT $n = 10$, 5xFAD $n = 11$. 8–10 months: student's t test, $p = 0.045$, WT n = 10, 5xFAD n = 8. 14 months: student's t test, $p = 0.036$, WT n = 8, 5xFAD n = 8. * $p < 0.05$. Data are expressed as mean ± SEM.
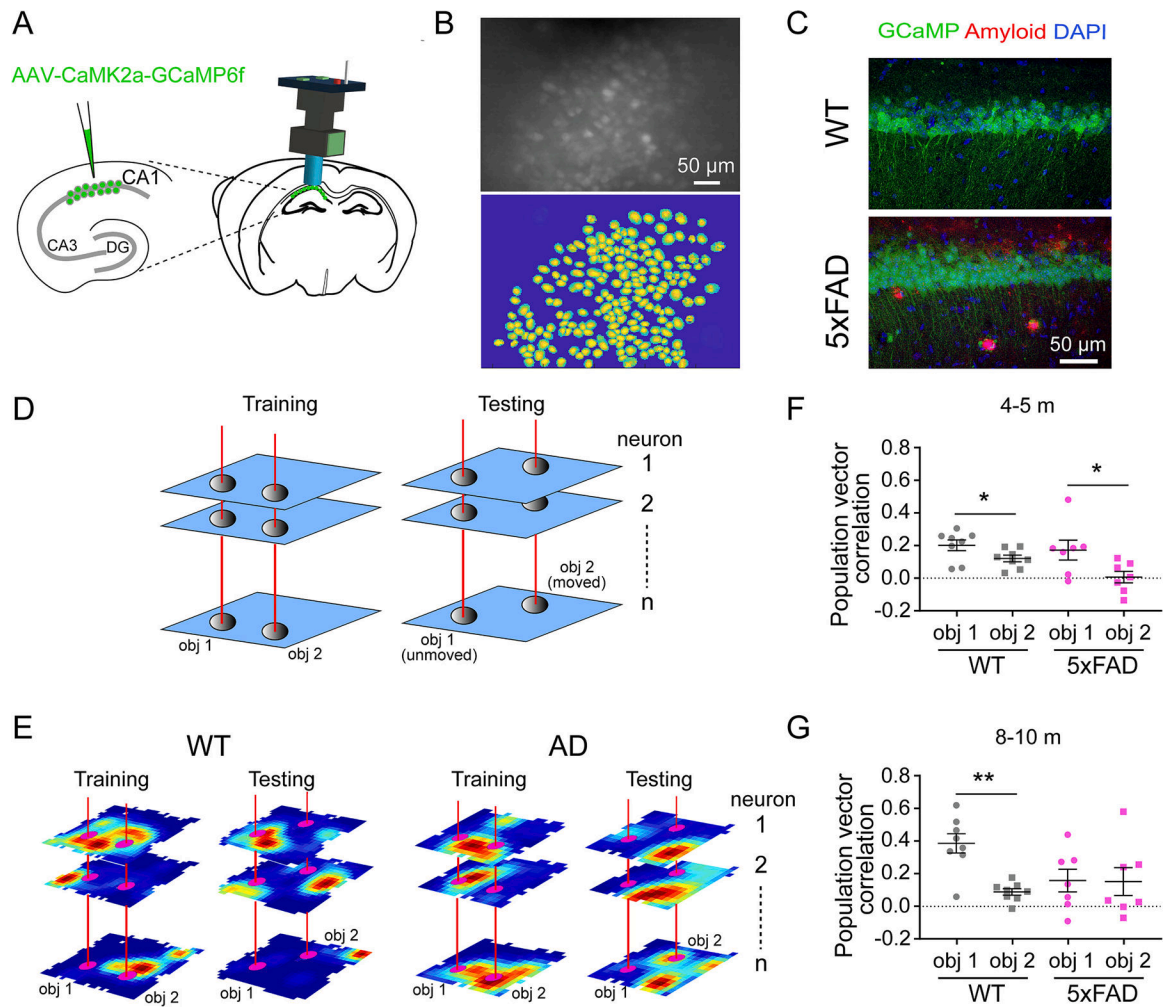
Fig. 2.

Impaired neural discrimination of object-location combinations in 5xFAD mice coincides with OLM deficits. A. Schematic of miniscope recording of CA1 calcium activity. AAV1-CaMk2a-GCamp6f was injected into dorsal CA1, then a GRIN lens was implanted above CA1 area to record calcium activity of CA1 neurons by a miniscope. B. A representative miniscope image of CA1 neurons (top) and extracted neuron footprints (bottom). C. Histological verification of AAV expression in CA1 pyramidal cell layer and amyloid aggregations in 5xFAD mice. D. Schematic of population vector correlation calculation. All rate maps of individual CA1 neurons from a single mouse were stacked into a 3-dimensional matrix with the spatial dimensions on the x and y axes and neurons on the z axis. The distribution of mean event rates along the z axis for each object location (within 3-bin distance surrounding the object) represents the population vector for that object. Then the correlation of population vectors between training and testing sessions was calculated for each object. E. Representative rate maps of 3 neurons for each genotype, which show the neural representation changes from training to testing sessions. F. Population vector correlations for each object at 4–5 months. Both WT (Mann-Whitney U test, $p = 0.038$, n = 8) and 5xFAD ($p = 0.0262$, $n = 7$) mice show significantly higher correlation for the unmoved object (obj1) than the moved object (obj2). G. Population vector correlations for

each object at 8–10 months. WT mice show significantly higher correlation for the unmoved object than the moved object ($p = 0.0047$, n = 8), while 5xFAD ($p = 0.71$, n = 7) mice show similarly low correlation for both objects. * $p < 0.05$, ** $p < 0.01$. Data are expressed as mean ± SEM.
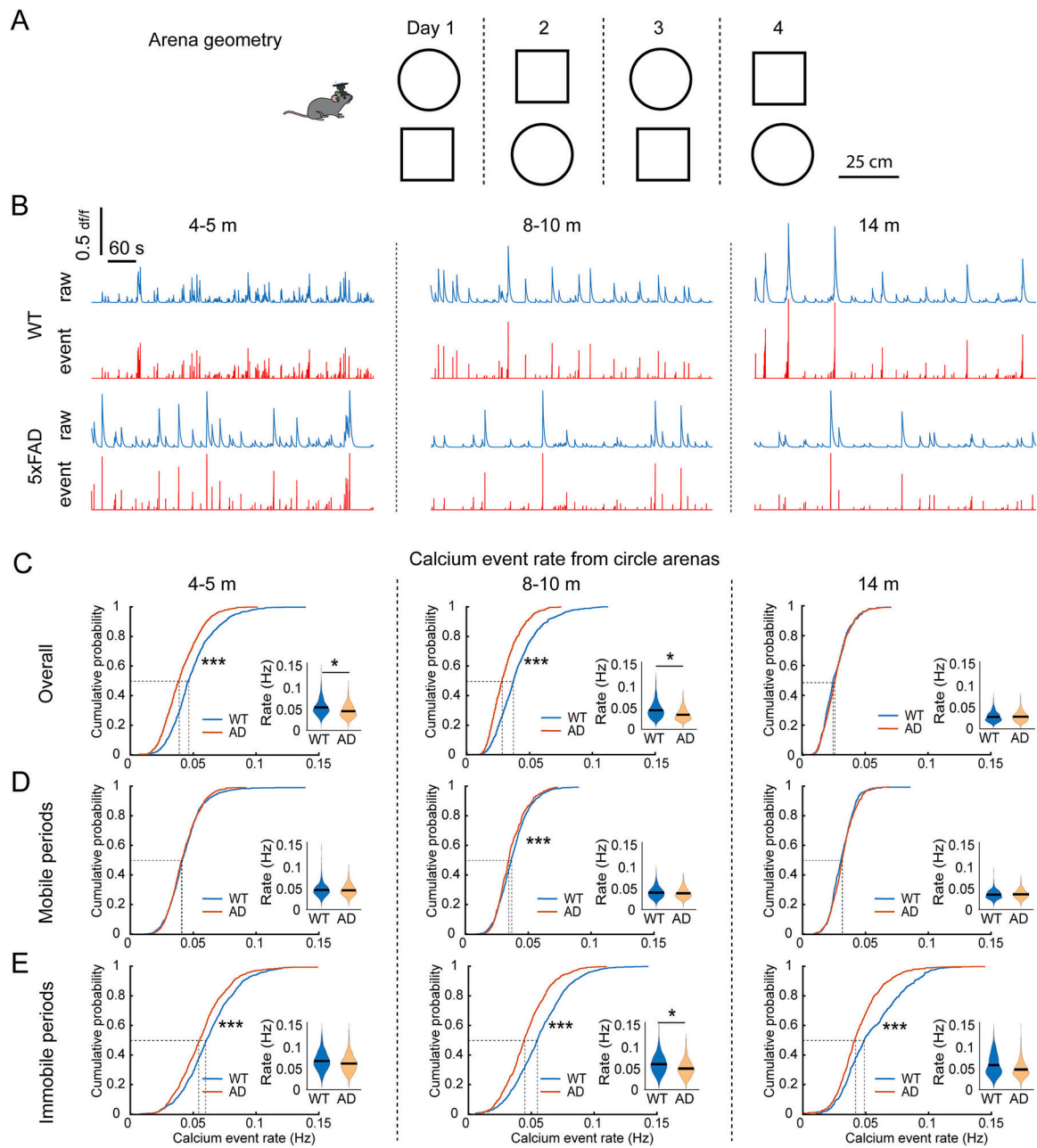
Fig. 3.

5xFAD mouse CA1 cells exhibit age-dependent changes in calcium event rate during mouse exploration of open field. A. Schematic of open field test. The test included 4 sessions in circle and square arenas each over 4 days. The order of circle and square was alternated every day. B. Representative calcium signal traces in the circle arena for WT and 5xFAD mice at 4–5, 8–10 and 14 months old. C. *Z*-scored calcium event rates during the overall session at different testing ages. CA1 neurons of WT mice show a gradually decreased event rate from 4 to 5 to 14 months, while 5xFAD mice lack this age-dependent change. K–S test for cumulative distributions: 4–5 months: $p = 3.68 \times 10^{-5}$, 8–10 months: $p = 4.22 \times 10^{-5}$, 14 months: $p = 0.997$. lme analysis for violin plots: 4–5 months: $p = 0.014$, 8–10 months:

p = 0.019, 14 months: $p = 0.99$. D. Z-scored calcium event rates during mobile periods of open field exploration. K–S test for cumulative distributions: 4–5 months: $p = 0.552$, 8–10 months: $p = 6.97 \times 10^{-4}$, 14 months: $p = 0.052$. lme analysis for violin plots: 4–5 months: $p = 0.562$, 8–10 months: $p = 0.318$, 14 months: $p = 0.787$. E. Z-scored calcium event rates during immobile periods. K–S test for cumulative distributions: 4–5 months: $p = 8.1 \times 10^{-8}$, 8–10 months: $p = 2.29 \times 10^{-19}$, 14 months: $p = 6.23 \times 10^{-15}$. lme analysis for violin plots: 4–5 months: $p = 0.277$, 8–10 months: $p = 0.048$, 14 months: $p = 0.125$. * $p < 0.05$, *** $p < 0.001$. n: 4–5-month: 812 neurons from 6 WT and 1034 neurons from eight 5xFAD; 8–10-month: 924 neurons from 9 WT and 672 neurons from seven 5xFAD; 14-months: 535 neurons from 5 WT and 898 neurons from five 5xFAD.
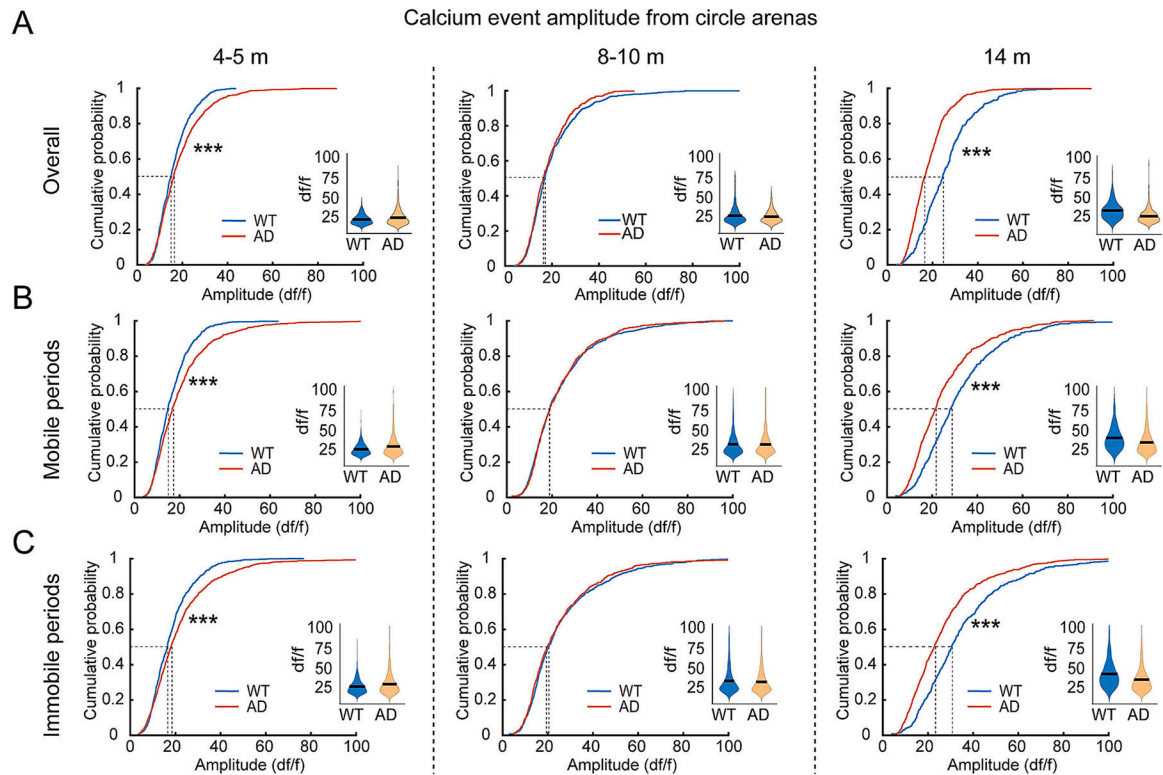
Fig. 4.

5xFAD mouse CA1 cells exhibit age-dependent changes in amplitudes of calcium events during mouse exploration of open field. A. Calcium event amplitudes of CA1 neurons during the overall session of exploring circular arena at different testing ages. CA1 neurons of WT mice show a gradually increased overall amplitude from 4 to 5 to 14 months, while 5xFAD mice lack this age-dependent change. K–S test for cumulative distributions: 4–5 months: $p = 1.67 \times 10^{-4}$, 8–10 months: $p = 0.32$, 14 months: $p = 2.17 \times 10^{-23}$. lme analysis for violin plots: 4–5 months: $p = 0.37$, 8–10 months: $p = 0.35$, 14 months: $p = 0.55$. B. Calcium event amplitudes of CA1 neurons during mobile periods. K–S test for cumulative distributions: 4–5 months: $p = 2.38 \times 10^{-7}$, 8–10 months: $p = 0.916$, 14 months: $p = 7.94 \times 10^{-15}$. lme analysis for violin plots: 4–5 months: $p = 0.297$, 8–10 months: $p = 0.862$, 14 months: $p = 0.884$. C. Calcium event amplitudes of CA1 neurons during immobile periods. K–S test for cumulative distributions: 4–5 months: $p = 1.74 \times 10^{-5}$, 8–10 months: p = 0.29, 14 months: $p = 5.44 \times 10^{-15}$. lme analysis for violin plots: 4–5 months: $p = 0.353$, 8–10 months: $p = 0.773$, 14 months: $p = 0.223$. *** p < 0.001. n: 4–5-month: 812 neurons from 6 WT and 1034 neurons from eight 5xFAD; 8–10-month: 924 neurons from 9 WT and 672 neurons from seven 5xFAD; 14-months: 535 neurons from 5 WT and 898 neurons from five 5xFAD.
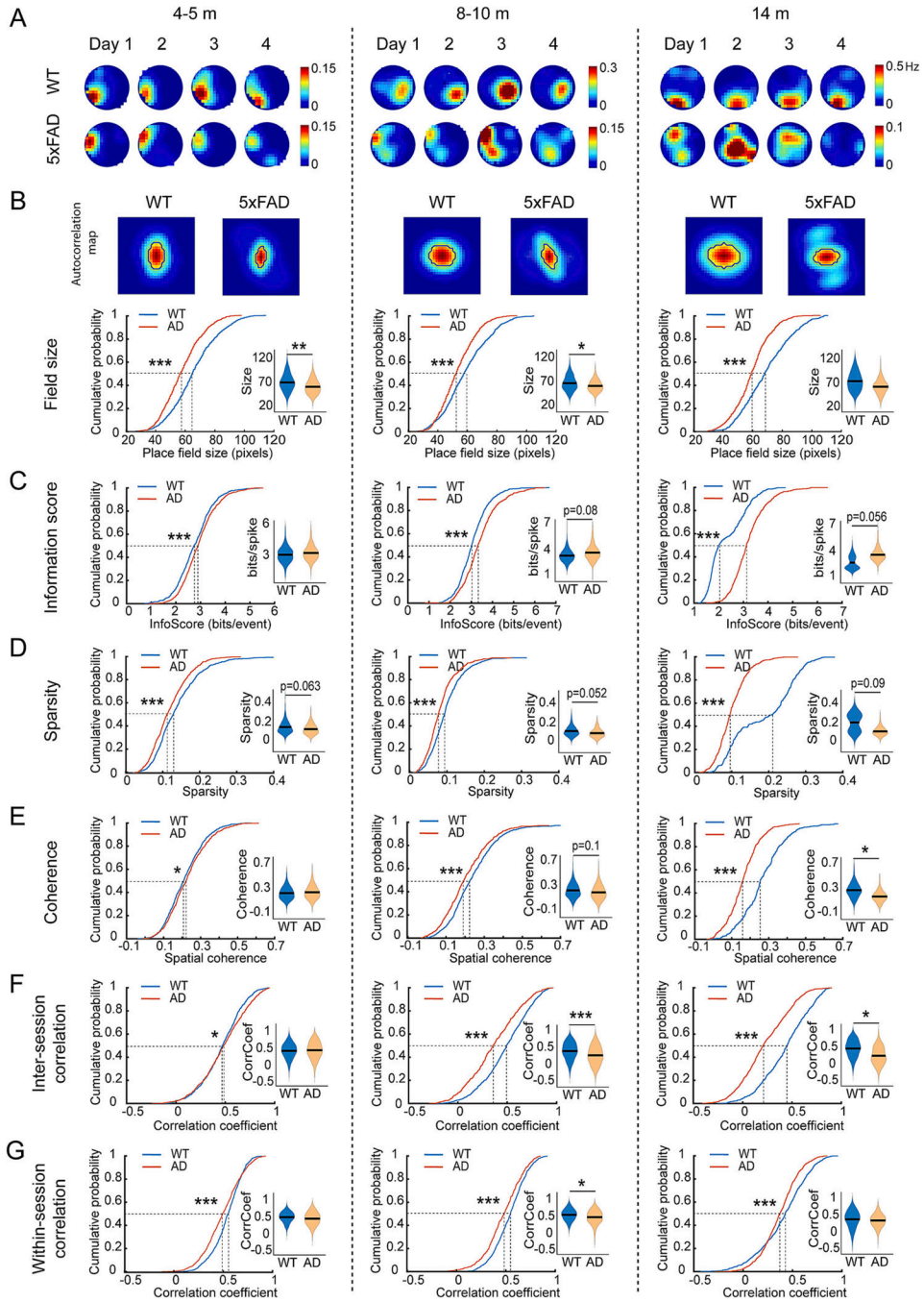
Fig. 5.

Degraded spatial tuning of CA1 neurons in open field precedes deficits in OLM in 5xFAD mice. A. Representative calcium event rate maps of individual CA1 neurons across the four sessions of mice exploring a circle arena at each testing age. The 4 rate maps at each age are from the same example neuron of WT or 5xFAD mice. B. Top, examples of autocorrelation rate maps. Bottom: CA1 neurons in 5xFAD mice show lower field size at all ages. K–S test for cumulative distributions: 4–5 months: $p = 6.51 \times 10^{-19}$; 8–10 months: $p = 9.45 \times 10^{-10}$; 14 months: $p = 1.25 \times 10^{-25}$. lme analysis for violin plots: 4–5 months: $p = 0.005$;

8–10 months: lme, $p = 0.029$; 14 months: $p = 0.21$. C. CA1 neurons in 5xFAD mice show higher information score (bits/events) at all ages. K–S test for cumulative distributions: 4–5 months: $p = 1.82 \times 10^{-4}$; 8–10 months: $p = 4.46 \times 10^{-9}$; 14 months: $p = 2.28 \times 10^{-55}$. lme analysis for violin plots: 4–5 months: $p = 0.18$; 8–10 months: $p = 0.08$; 14 months: $p = 0.056$. D. CA1 neurons in 5xFAD mice show lower sparsity at all ages. K–S test for cumulative distributions: 4–5 months: $p = 2.29 \times 10^{-5}$; 8–10 months: $p = 6.25 \times 10^{-8}$; 14 months: $p = 6 \times 10^{-53}$. lme analysis for violin plots: 4–5 months: $p = 0.063$; 8–10 months: lme, $p = 0.052$; 14 months: $p = 0.09$. E. CA1 neurons of 5xFAD mice show slightly higher spatial coherence at 4–5 months but greatly lower after 8 months. K–S test for cumulative distributions: 4–5 months: $p = 0.043$; 8–10 months: $p = 8.11 \times 10^{-5}$; 14 months: $p = 3.98 \times 10^{-40}$. lme analysis for violin plots: 4–5 months: $p = 0.29$; 8–10 months: $p = 0.1$; 14 months: $p = 0.029$. F. CA1 neurons of 5xFAD mice show slightly higher inter-session correlation of rate maps at 4–5 months but greatly lower after 8 months. K–S test for cumulative distributions: 4–5 months: $p = 0.0019$; 8–10 months: $p = 2.21 \times 10^{-16}$; 14 months: $p = 1.69 \times 10^{-31}$. lme analysis for violin plots: 4–5 months: $p = 0.222$; 8–10 months: $p = 6.83 \times 10^{-5}$; 14 months: $p = 0.031$. G. CA1 neurons of 5xFAD mice show decreased within session reliability at all ages. K–S test for cumulative distributions: 4–5 months: $p = 3.29 \times 10^{-10}$; 8–10 months: $p = 1.15 \times 10^{-7}$; 14 months: $p = 4.24 \times 10^{-9}$. lme analysis for violin plots: 4–5 months: $p = 0.147$; 8–10 months: $p = 0.047$; 14 months: $p = 0.134$. * $p < 0.05$, ** $p < 0.01$, *** $p < 0.001$. n: 4–5-month: 812 neurons from 6 WT and 1034 neurons from eight 5xFAD; 8–10-month: 924 neurons from 9 WT and 672 neurons from seven 5xFAD; 14-months: 535 neurons from 5 WT and 898 neurons from five 5xFAD.
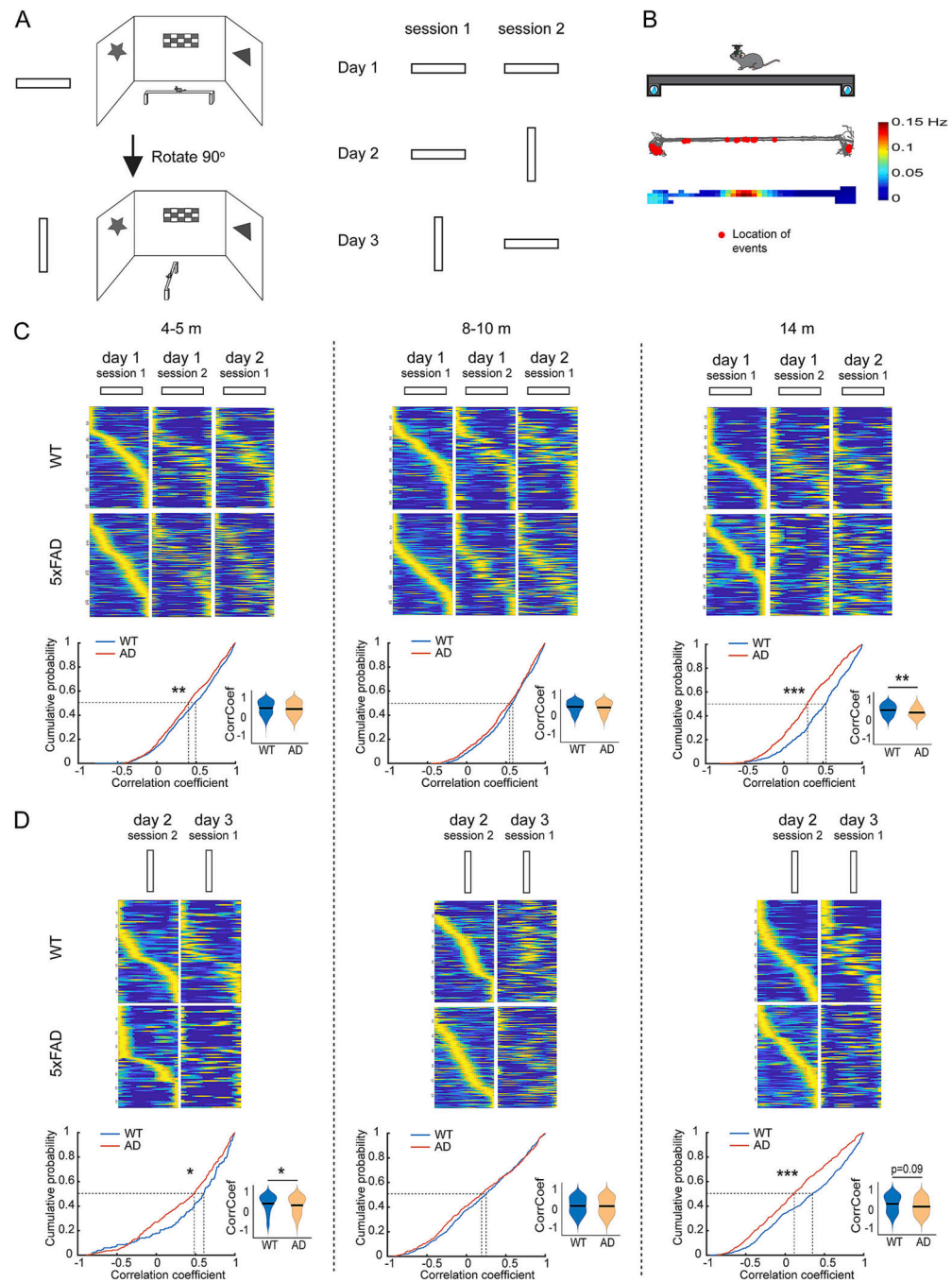
Fig. 6.
Unstable spatial encoding during linear track test in 5xFAD mice precedes OLM deficit. A. Schematic of linear track test which includes 6 sessions of 2 different orientations spreading in 3 days. B. Mouse movement trajectory of an example session and locations of calcium events of an example neuron. Mouse trajectory is illustrated in gray lines and the red dots indicate the locations of calcium events. The quantitative color-coded rate map is shown in the bottom by the color scale. C. 5xFAD mice show decreased inter-session rate map correlations across the first three sessions of the same orientation. Example rate maps shown

in top panels are sorted by the order of the peak calcium event rate in the first session for each time point. Bottom: K–S test for cumulative distributions: 4–5 months: $p = 0.007$; 8–10 months: $p = 0.161$; 14 months: $p = 1.95 \times 10^{-10}$. lme analysis for violin plots: 4–5 months: p = 0.99; 8–10 months: p = 0.99; 14 months: $p = 0.007$. D. 5xFAD mice show decreased inter-session rate map correlation between the two sessions of rotated orientation. Rate maps shown in top panels are sorted by the order of the peak calcium event rate in the first session for each time point. Bottom: K–S test for cumulative distributions: 4–5 months: p = 0.043; 8–10 months: $p = 0.508$; 14 months: $p = 3.17 \times 10^{-6}$. lme analysis for violin plots: 4–5 months: $p = 0.037$; 8–10 months: $p = 0.87$; 14 months: p = 0.09. ** p < 0.01, *** p < 0.001. n: 4–5-month: 943 neurons from 9 WT and 736 neurons from seven 5xFAD; 8–10-month: 663 neurons from 9 WT and 566 neurons from six 5xFAD; 14-months: 515 neurons from 6 WT and 506 neurons from five 5xFAD. (For interpretation of the references to color in this figure legend, the reader is referred to the web version of this article.)
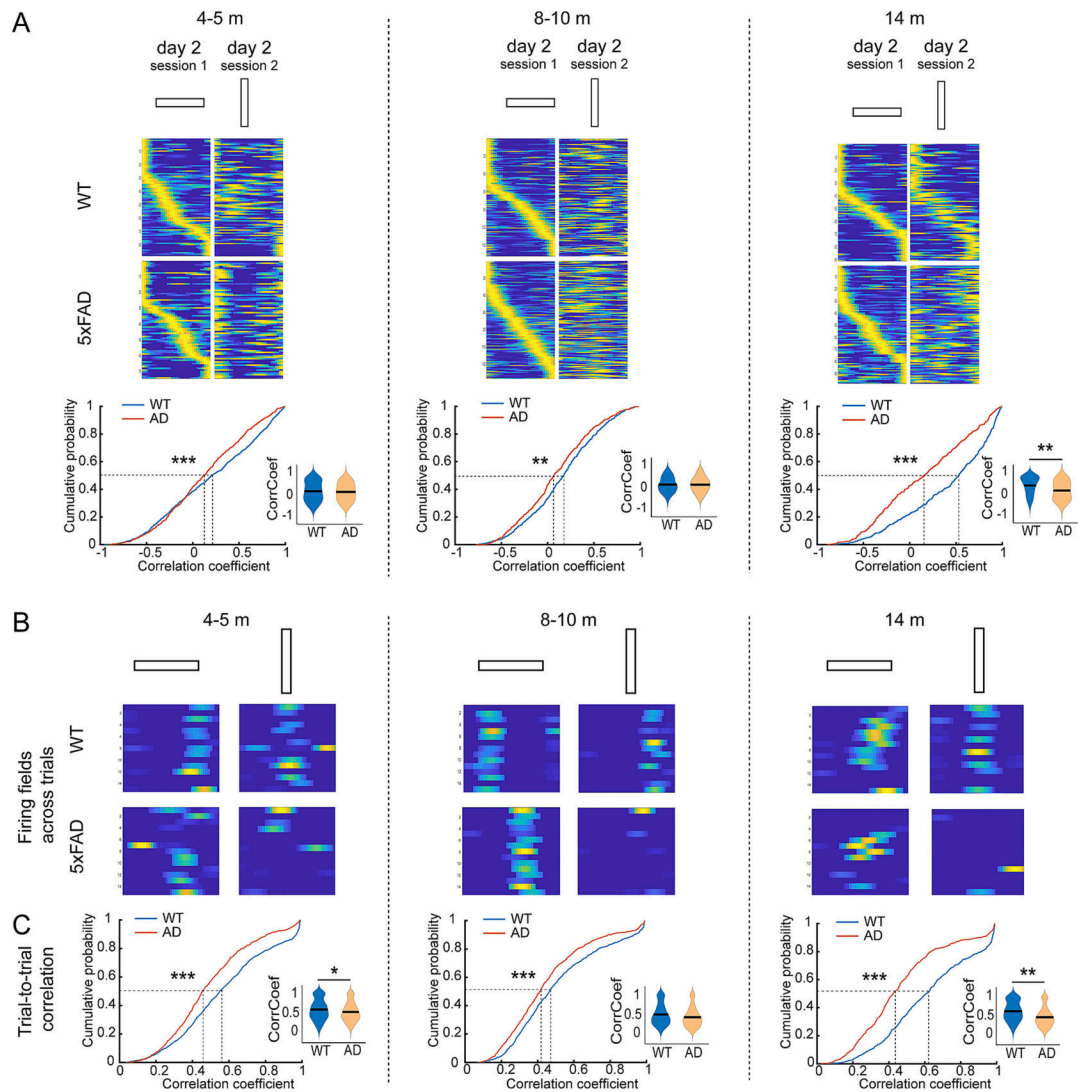
Fig. 7.

5xFAD CA1 neurons show unreliable within-session trial-to-trial location tuning on linear track starting at 4–5 months old. A. 5xFAD mice show lower inter-session rate map correlation between the two sessions of different orientations. Rate maps shown in top panels are sorted by the order of the peak calcium event rate in the first session for each time point. Bottom: K–S test for cumulative distribution: 4–5 months: $p = 1.73 \times 10^{-5}$; 8–10 months: p = 0.001; 14 months: $p = 6.11 \times 10^{-14}$. lme analysis for violin plots: 4–5 months: $p = 0.92$; 8–10 months: p = 0.18; 14 months: $p = 0.0027$. B. Within session trial by trial plot of activy fields of example neurons from a WT or 5xFAD mouse at each recording age, and the fields from trials of initial and rotated orientations are shown. C. CA1 neurons of 5xFAD mice show significantly decreased trial-to-trial reliability at all ages. K–S test for cumulative distribution: 4–5 months: $p = 9.36 \times 10^{-8}$; 8–10 months: $p = 1.33 \times 10^{-4}$; 14 months: p = 1.73×10^{-25}. lme analysis for violin plots: 4–5 months: p = 0.031; 8–10 months: 0.155; 14 months: $p = 0.0017$. * p < 0.05, ** p < 0.01, *** p < 0.001. n: 4–5-month: 943 neurons from 9 WT and 736 neurons from seven 5xFAD; 8–10-month: 663 neurons from 9 WT and 566

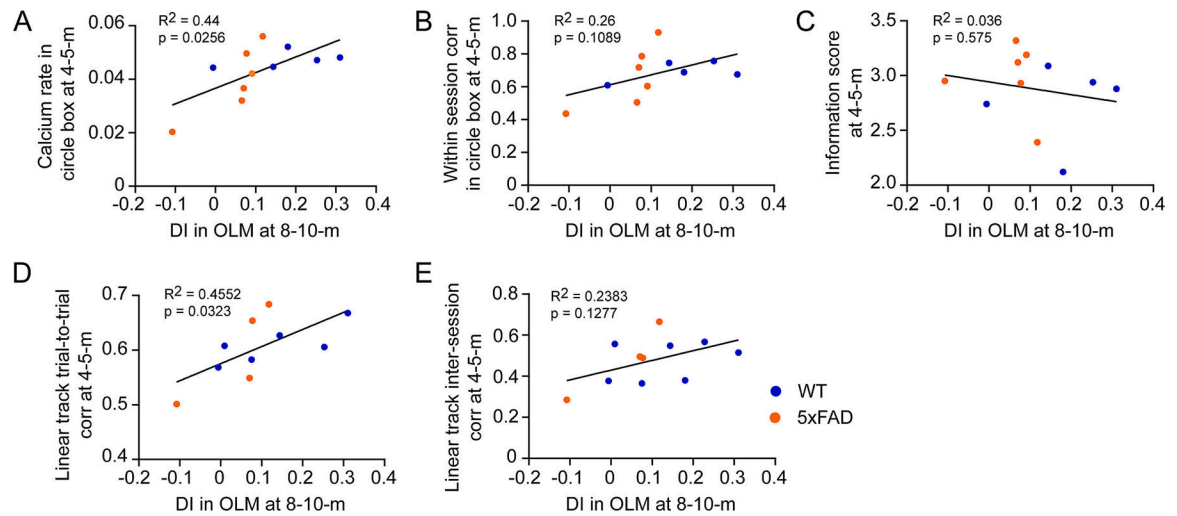neurons from six 5xFAD; 14-months: 515 neurons from 6 WT and 506 neurons from five 5xFAD.

Fig. 8.

Suppressed CA1 neuron calcium activity and unreliable spatial encoding at early stage predict OLM deficit at older age. A. Correlation between calcium event rate at 4–5-month and DI in OLM test at 8–10-month of individual animals. B. Correlation between within-session stability in circle box at 4–5-month and DI in OLM test at 8–10-month of individual animals. C. Correlation between information score at 4–5-month and DI in OLM test at 8–10-month of individual animals. D. Correlation between trial-to-trial stability in linear track at 4–5-month and DI in OLM test at 8–10-month of individual animals. F. Correlation between inter-session stability in linear track at 4–5-month and DI in OLM test at 8–10-month of individual animals.